Proceedings of ASME Turbo Expo 2004
Power for Land, Sea, and Air
June 14-17, 2004, Vienna, Austria

GT2004-53650

A COMPARATIVE AERODYNAMIC AND PERFORMANCE STUDY OF A THREE-STAGE HIGH PRESSURE TURBINE WITH 3-D BOWED BLADES AND CYLINDRICAL BLADES

M. T. Schobeiri/Professor
*TPFL:*Turbine Performance and Flow Research Laboratory
Texas A&M University
College Station, Texas 77843-3123, USA

A. Suryanarayanan/Research Assistant
*TPFL:*Turbine Performance and Flow Research Laboratory
Texas A&M University
College Station, Texas 77843-3123, USA

C. Jermann/Research Assistant [1]
Swiss Federal Institute of Technology
Zurich, Switzerland

T. Neuenschwander/Research Assistant [1]
Swiss Federal Institute of Technology
Zurich Switzerland

ABSTRACT

To investigate the effect of the blade geometry on blade total pressure loss coefficient, efficiency, and performance, a comparative study is presented that deals with the aerodynamic and performance behavior of a three-stage high pressure research turbine utilizing two different blade types. Keeping the initial conditions and the pressure ratio the same, two different rotors with the same hub and tip diameters are experimentally investigated. The first rotor incorporates 3-D convexly bowed blades, where as the second one utilizes a set of fully cylindrical blades. Using shrouded rotors and stators, the stator rings are correspondingly configured. The research turbine incorporates six rows beginning with a stator row. Interstage aerodynamic measurements are performed at design speeds at three stations, namely downstream of the first rotor row, the second stator row, and the second rotor row. For both rotors, the interstage radial and circumferential traversing present detailed flow pictures of the middle stage. Aerodynamic measurements were carried out at the turbine design speed. The experimental investigations have been carried out on a HP 3-stage gas turbine research facility at the Turbomachinery Performance and Flow Research Laboratory of Texas A&M University.

INTRODUCTION

Aerodynamic analysis of high pressure turbines is a continually evolving field with newer and accurate findings emerging due to improved measurement techniques and better instrumentation. The results of such analyses are oriented towards providing the design engineer with sufficient information to put forward an improved design that would facilitate higher machine efficiencies. One of the primary causes leading to the loss of efficiency in a turbomachine is the secondary flow which occurs at the rotor tip and the hub region. The flow near the blade tip and hub generates vortices which induce drag forces that reduce the total pressure of the fluid over the blades. Similarly the boundary layer and high and low pressure fluid mixing near the rotor hub also influence the flow near the hub, slowing it down and increasing the losses. The magnitude of losses and performance at both these locations depends to a great extent on the geometry of the blade. The losses are significant especially in the case of high pressure turbines with small aspect ratios. Hence to quantify the effects of blade geometry on the aerodynamic characteristics of flow in HP turbines, two different blade geometries namely, cylindrical blades and 3-D bowed blades are tested under similar test conditions. Reduction in the losses in these secondary zones can result in major energy savings. Several attempts have been made earlier to understand the nature of

[1] Performed their Diplomarbeit at *TPFL*

secondary flow and their effects on the performance of turbines.

In an experimental study on a multistage low-pressure (LP) turbine, Arndt [1] illustrated the profound influence of the wake-induced rotor-stator and rotor-rotor interaction on the flow through downstream blade rows. Arndt showed that the interaction results in strongly amplitude-modulated periodic and turbulent velocity fluctuations downstream of every rotor blade row. Sieverding [2] carried out a thorough study of the secondary flows in turbine blade passages using a turbine cascade test facility. Bindon [3] theorized the mechanisms involved in the generation of losses in turbines due to secondary flows also using turbine cascades. Chana and Jones [4] conducted experiments to quantify the heat transfer and static pressure distributions at the rotor tip and casing of a gas turbine. They found that the heat transfer changed significantly when the inlet temperature profile was varied from a uniform to a non uniform distribution. Non-uniform temperature distribution gave rise to smaller thermal loading near the rotor tip and casing areas. It was observed that the static pressures exhibited only slight fluctuations with variation in inlet temperature profile.

Schobeiri et al. [5] determined the stage-wise aerodynamic parameters. The tests were conducted on a high pressure 3-stage research turbine with 3-D bowed blades. A rotor speed range between 75% to 116% of the design speed was studied so as to understand the off-design performance of the turbine. A large decrease in the efficiency for speeds lower than the design speed was reported. But interestingly for rotor speeds greater than the design speed the efficiencies increased. It was found that the 3-D blades used caused a high axial velocity near the rotor hub and the tip, thereby subduing the losses due to secondary and tip vortices.

Aunapu et al. [6] presented methods to divert secondary flow in order to allow for increased turbine inlet temperatures. In general it was observed that the redirection of the secondary flow increased the effectiveness of the film cooling. Prasad and Wagner [7] documented the characteristics of the unsteady flow between the turbine blade tip and the air seal. They noticed a vena contracta structure appearing in the clearance region due to the separation of flow at the rotor tip.

Camci et al. [8] investigated the effects of squealer rims on the aerodynamic characteristics of a turbine stage. It was reported that the squealer rings were found to be effective in reducing the effects of the tip leakage more so when designed on the suction side of the blades. They also studied the effects of redirecting a part of the tip leakage flow over the trailing edge through different channels to subdue the tip vortices. The suction side squealers provided the best leakage flow sealing even when compared to the tip flow diversion methods.

The characteristics of the flow in a rotor or a stator are affected by the vortex created by the upstream blades. Chaluvadi et al. [9]. examined the consequences of delta wing vortex transport on the 3-D flow field within the blade rows of a HP steam turbine. Tests were conducted with and without delta wing configurations to understand the variations the delta wings cause inside the flow field. The delta wings caused steep increase in total pressure loss when compared with the basic configuration. The nature of the rotor exit flow when subjected to the vortices from the upstream stator and the rotor itself was also studied. The flow variations at the rotor exit due to the upstream stator was similar to the fluctuations undergone by the stator due to the presence of the half delta wings. It was also noted that the stagnation pressure at the rotor exit showed little variation between the datum case and the half delta wing configuration.

Recent experimental and theoretical studies have indicated that blades with compound lean contribute towards reducing the secondary flow losses thereby improving the turbine efficiencies (Schobeiri et al. [5], Staubach et al. [10], Walker [11]). Advancements in 3-D flow field calculation methods have enabled accurate prediction of the nature of complex flows and have allowed for the extensive usage of sweep and lean features in blade design. The 3-D blade profiles utilized for this study shown in Fig. 6 are modified cylindrical blade profiles but with accentuated blade sweep and compound lean. Since the cylindrical blades (Fig. 7) are usually designed to operate at mid-height radius with optimum efficiency, they do not account for the radial equilibrium. Thus, any deviation from that radius causes incidence changes that are associated with increased total pressure losses. At the hub and tip regions a strong incidence change contributes to strengthening the secondary flow vortices thus increasing the secondary flow losses. The introduction of 3-D blades with compound lean (Fig. 6) counteracts the secondary vortices causing a reduction in secondary flow losses. The effectiveness of blade lean and sweep in reducing the secondary flow losses are discussed in detail by Denton and Xu [12].

The current study attempts to quantify the secondary flow loss reduction with blade geometries by comparing the experimental results obtained from detailed interstage pressure measurements of a HP 3-stage turbine with cylindrical and 3-D bowed blade configuration. The tests were conducted at the rotor design speed of 2600rpm and a mass flow rate of 3.728kg/s.

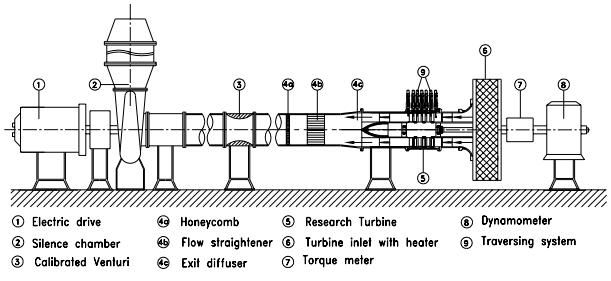

Figure 1 3-Stage HP turbine facility at *TPFL*, TAMU.

NOMENCLATURE

CT Circumferential traverse
n Rotational speed [rpm]

p Static pressure [kPa]
P Total pressure [kpa]
r^* Immersion ratio, $(r-r_{hub})/(r_{tip}-r_{hub})$
RT Radial traverse
α Absolute flow angle [^{0}]
β Relative flow angle [^{0}]
ζ Total pressure loss coefficient [-]
$\zeta_{0.5}$ Total pressure loss coefficient at blade mid-height

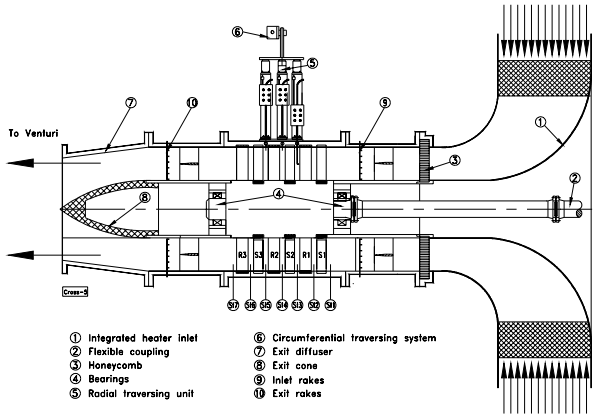

Figure 2 Cross section of the HP turbine and its major components.

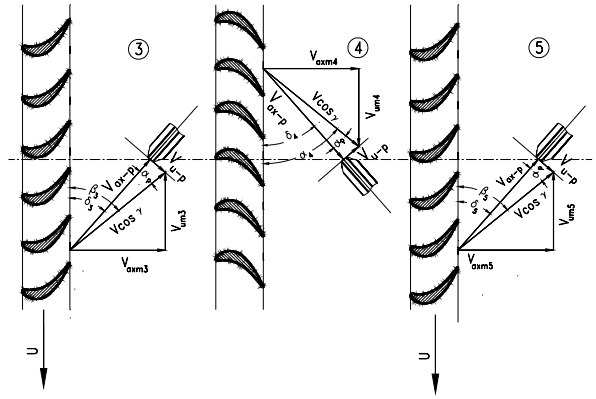

Figure 3 Angular position of the 5-hole probe at the three stations

EXPERIMENTAL FACILITY

The overall layout of the test facility is shown in Fig.1 It consists of ① A 300-kW electric motor connected to a frequency controller which drives the compressor component. ② A three-stage centrifugal compressor supplies air with a maximum pressure difference of 55kPa and a volume flow rate of 4 m^3/s. The compressor operates in suction mode and its pressure and volume flow can be varied by a frequency controller from 0 to 66Hz. The compressor and its drive are located inside a housing which is outside the test cell. A pipe with a transition piece connects the compressor to a Venturi mass flow meter ③ used to measure the mass flow through the turbine component. ④ The exit diffuser serves as a smooth transition piece between the turbine component and the Venturi, which is used for mass flow measurement. ⑤ The three-stage turbine with fully automated data acquisition system is the core component of the test facility. ⑥ The turbine inlet has an integrated heater that prevents condensation of water from humid air expanding through the turbine during the test. ⑦ The turbine shaft is connected through a flexible coupling with one end of a high precision torque meter that has a maximum rotational speed of 8500 rpm and a maximum torque of 677.9 N-m. The other end of the torque meter is coupled via a second flexible coupling with an eddy current low inertia dynamometer ⑧with a maximum power capacity of 150 kW and a maximum torque of 500Nm.

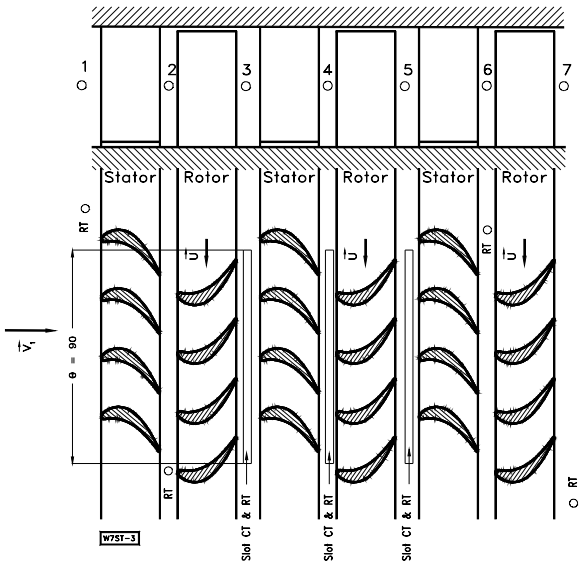

Figure 4 Axial Location of stations 3, 4 and 5.

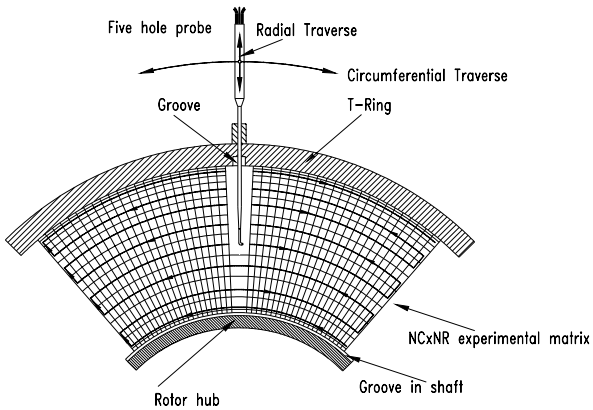

Figure 5 Radial and Circumferential measurement grid NCxNR.

Interstage Instrumentation

The turbine component shown in Fig. 2 is a three-stage air turbine with the dimensions and operating conditions specified in Table 1. To achieve a high degree of versatility, the turbine was designed with a casing that incorporates stator rings. It also incorporates three T-rings

for sealing the three 90-degree circumferential traversing slots, as seen in Figs. 2 and 3. The sealed T-rings move circumferentially inside the slots shown in Fig. 4 and effectively prevent the leakage of mass flow through the slots. As shown in Figs. 1 and 3, three five-hole probes are mounted on three traversing systems with decoder and encoder for accurate probe positioning. The traverse in the radial direction spans from 1mm below the hub diameter to 1mm above the blade tip. The measurement grid for the data acquisition is shown in Fig. 5. N_r and N_c are the number of radial and circumferential locations at which the measurements are made.

Performance Instrumentation

For the performance instrumentation, combined total pressure, total temperature rakes are used upstream of the first stator row and downstream of the last rotor row. At the inlet, the rakes were located radially at 45^o, 135^0, 225^o, and 315^o. Each rake consists of 4 total pressure and 3 total temperature probes that are equidistantly distributed in the radial direction. The total pressure probes are of the Pitot tube types, and the total temperature probes are calibrated J-type thermocouples. To reduce the wake thickness originating from the trailing edge of the inlet rakes, the rakes are shaped aerodynamically with a round leading edge and a sharp trailing edge.

Item	Specification	Item	Specification
Stage no.	N = 3	Mass flow	ms =3.728 kg/s
Tip diam.	D_t = 685.8mm	Speed range	n =1800-2800rpm
Hub diam.	D_h =558.8mm	Inlet pressure	p_{in} = 101.356 kPa
Blade height	Bh = 63.5 mm	Exit pressure	p_{ex} = 71.708 kPa
Blade no.	Stator 1 = 58	Stator 2 = 52	Stator 3 = 56
Blade no.	Rotor 1 = 46	Rotor 2 = 40	Rotor 3 = 44
Power	P = 80.0-110.0 kW		

Table 1 : Turbine research facility data.

The exit rakes are located radially with the same spacing as the inlet rakes, but offset to them in order to prevent the interference with the inlet rake wakes. Wall static pressure taps are arranged at the top and bottom half of the main casing and on the T-rings, as well as on the stator rings. In addition, total temperature and pressure probes are mounted on the leading edge stagnation points of two diametrically opposed stator blades of the second and third stator rows.

The turbine facility has the capability of radially traversing the flow field at stations 1 through 7 (Fig. 3) and circumferentially/ radially traversing at stations 3, 4, and 5. The data from the traversing is used to generate the total and static pressure contours, velocity components, flow angles and the span wise distribution of total pressure loss coefficients and the efficiency for each row. For this purpose, three L-shaped five-hole probes were used. The first and the third probes were installed at stations 3 and 5 and were calibrated at low subsonic Mach number (M = 0.1), while the second one installed at station 4 was calibrated taking into account any small compressibility effects due to the moderate subsonic Mach number of M = 0.3.

A non-nulling calibration method was applied. The five-hole probes were independently calibrated in a fully automated calibration facility. Each one of the probes were placed in an angular indexing mechanism and then was pitched and yawed through the range of angles (-20^0 to 20^0 in pitch and -30^0 to 30^0 in yaw) in 2 degree increments. The calibration facility probe indexing mechanism uses two stepper motors that are computer controlled to achieve a very fine angle resolution. A computer algorithm that creates a user-specified grid of pitch and yaw angles is used to control these stepper motors. The same algorithm also records the pressures from the PSI- 9016 pressure scanner and puts the pressures from the five-hole probe with the corresponding pitch and yaw angles and the calibration nozzle total pressure into a data file. This data file is then used to create the calibration surfaces for the specific probes that are later used to determine the velocity components and vectors at stations 3, 4, and 5 of the turbine engine. The three probes are turned at specified angles δ_3, δ_4, and δ_5

Figure 6 3-D bowed blades mounted on the cylinder.

Figure 7 Cylindrical blades mounted on the cylinder.

(Fig. 2). The absolute and relative flow angles and velocity components of the turbine rows are calculated by implementing the probe adjustment angle δ_i for each of the three probes at stations 3,4 and 5 respectively.

Rotors used for Comparative Study

To investigate the effects of the blade geometry on blade total pressure loss coefficient, efficiency, and performance, two rotor units with the same hub and tip diameters but different blade types are utilized. The first rotor incorporates 3-D convexly bowed blades, Fig. 6, whereas the second utilizes a set of fully cylindrical (2-D) blades, Fig. 7. Using shrouded rotors and stators, the stator rings are correspondingly configured. Keeping the initial conditions and the pressure ratio the same, both the rotors are experimentally investigated. The rotor blades are shrouded and attached to the rotor cylinder, which is connected to the shaft via two locking mechanisms. This design allows to disassemble the entire rotor unit and to reuse the shaft and the bearings, when replacing the cylinder for another turbine type. The versatile turbine design allows clocking the stator rings individually and externally without disassembling the turbine.

RESULTS AND DISCUSSION

Interstage traversing was performed at stations 3, 4 and 5 and pressure readings were acquired using five hole probes. The radial flow parameters are plotted against a non-dimensional ratio defined as the immersion ratio,r*:

$$r* = (r-r_h)/(r_t-r_h) \quad (1)$$

The acquired data is consistently averaged following the consistent averaging method specified by Dzung [13]. This method of averaging complies with the conservation laws of thermodynamics and fluid mechanics and is appropriate for analyzing turbomachinery data. The turbine was operated at its design speed of 2600rpm and aerodynamic

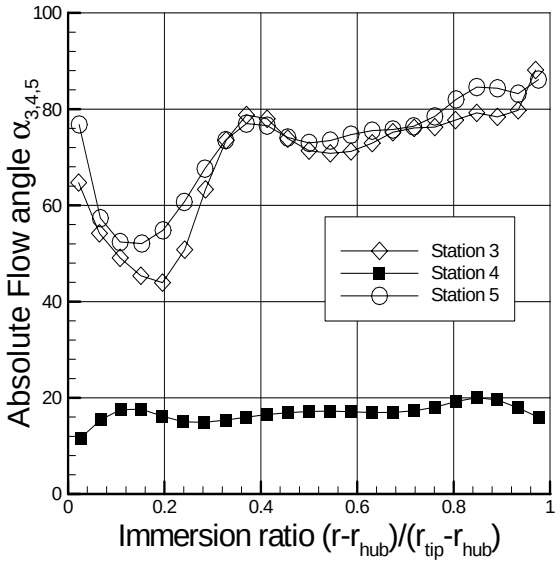

Figure 8 Radial distribution of absolute flow angle, Cylindrical blades - 2600rpm.

flow measurements were made for the two blade configurations described earlier.

Flow angle distribution

The absolute flow angle (α) as a function of the immersion ratio, r*, for the cylindrical and 3-D bowed blades is shown in Fig. 8 and 9 respectively. The direction of flow at station 4 which is at the stator exit shows small variations for the two blades. The flow at this station follows the stator blade metal exit angle and is approximately 19° for the cylindrical blades with the corresponding deviation between 15° and 20° for the 3-D bowed blades. At stations 3 and 5, which are at the rotor exit, the flow is observed to change directions continuously. For the cylindrical blades between r*=0.0 and 0.4, the absolute flow angle falls to 45° before increasing rapidly to about 80°. Beyond this region of large variation close to the blade root, the angle increases gradually to 90° at the blade tip. In the case of the 3-D blades the initial dip and rise seen

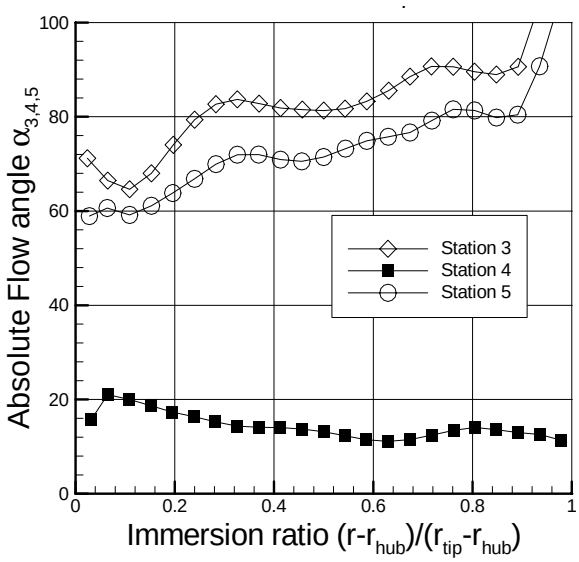

Figure 9 Radial distribution of absolute flow angle, 3-D Bowed blades - 2600rpm.

for the cylindrical blades between r*=0.0 and 0.4 is absent. It appears that the flow is not greatly affected by the low energy boundary layer flow near the hub wall and undergoes only small directional changes. The 3-D blades also exhibit similar absolute flow angle between r*=0.4 and the blade tip like the cylindrical blades. Also for the 3-D bowed blades the absolute flow angle at station 5 is consistently smaller than at station 3 by approximately 5°.

Fig. 10 and 11 represent the radial distribution of the relative flow angle, β, for the cylindrical and 3-D blades respectively. The relative flow angles at stations 3 and 5 show moderate to zero variations and remain around 20° irrespective of the blade geometry. For the cylindrical blades at station 4 the relative flow angle increases continuously till the blade tip and is greater than at stations 3 and 5. In contrast, the results for the 3-D bowed blades indicate three distinct regions of the relative flow angle variations at station 4. Between r*=0.0 to 0.25 the flow sees

a decrease in the relative flow angle, while remaining unchanged at 50° between r*=0.25 and 0.6. Beyond r*=0.6 the relative flow angle increases up to the blade tip.

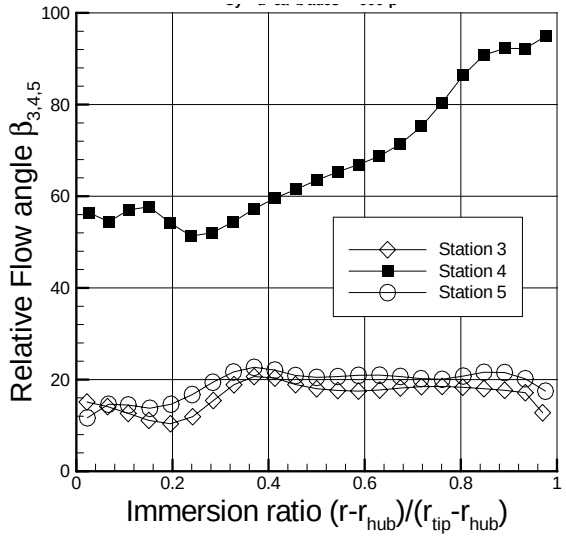

Figure 10 Radial distribution of relative flow angle, Cylindrical blades - 2600rpm.

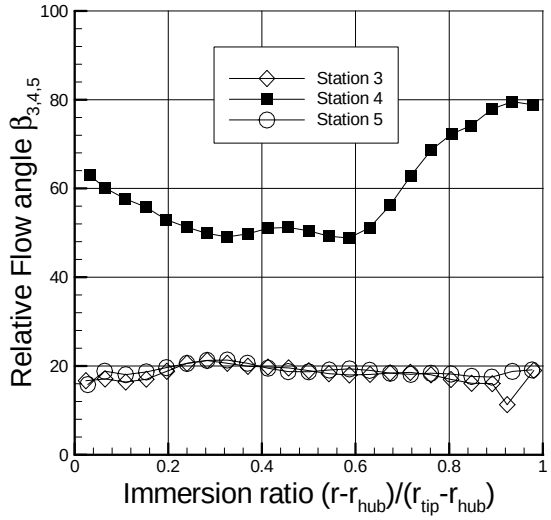

Figure 11 Radial distribution of relative flow angle, 3-D Bowed blades - 2600rpm.

Mach number and axial velocity distribution

The radial distribution of absolute Mach number for the two blade configurations are shown in Figs. 12 and 13 respectively. For both the blade geometries it is seen that the absolute Mach numbers at stations 3 and 5 remain subsonic and well under the compressible flow limit and between 0.07-0.1. For the cylindrical as well as the 3-D bowed blades the absolute Mach numbers at station 4 which is downstream of the second stage stator, the flow experiences higher velocities, pushing the compressible flow limit, up to 2/3rds of the blade length. Again at station 4 the velocities, affected by the tip secondary flow decreases slightly as we proceed towards the blade tip for the two blade profiles. The situation reverses for the relative Mach number distribution (Fig. 14,15) where the rotor exits (stations 3,5) encounter higher Mach numbers than the stator exit (station 4) for both the blades.

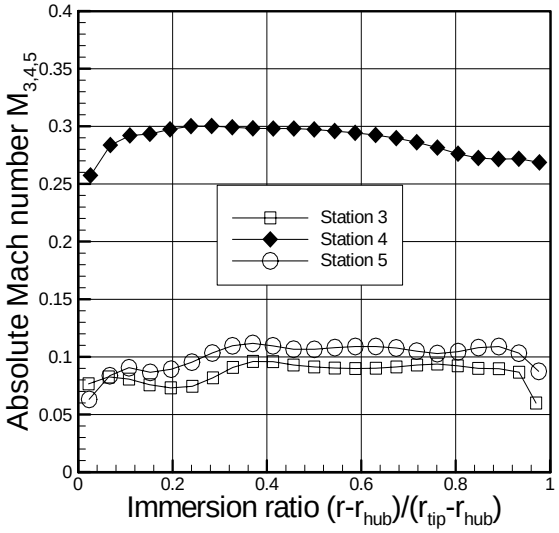

Figure 12 Radial distribution of absolute Mach number, Cylindrical blades - 2600rpm.

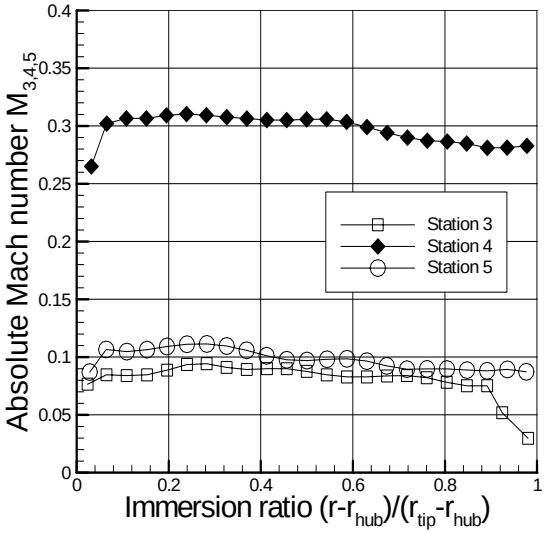

Figure 13 Radial distribution of absolute Mach number, 3-D Bowed blades - 2600rpm.

A comparison of Fig. 14 and 15 indicates that the blade geometry seems to have little influence on the relative Mach number distribution in the radial direction. The axial velocity distribution is shown in Figs. 16 and 17 for both the cylindrical and the 3-D bowed blades as a function of the immersion ratio. The axial velocity for the cylindrical blades (Fig. 16) close to the rotor hub is affected greatly by the interaction of the secondary flow at the hub with the main turbine channel flow. This effect manifests as reduced axial velocities up to r*=0.15 at station 4 and up to r*=0.25 at stations 3 and 5.

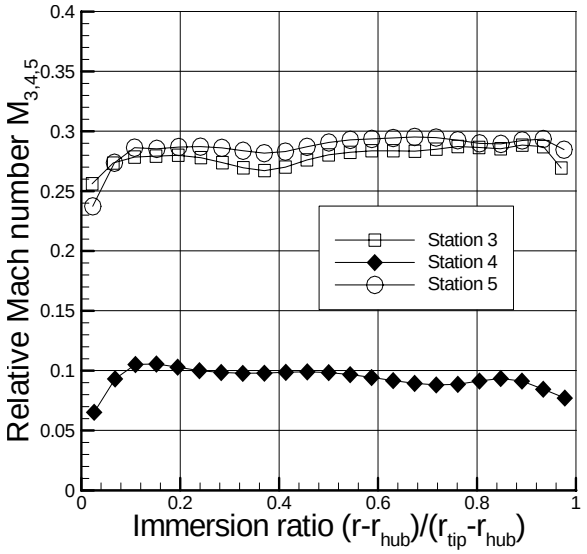

Figure 14 Radial distribution of relative Mach number, Cylindrical blades - 2600rpm.

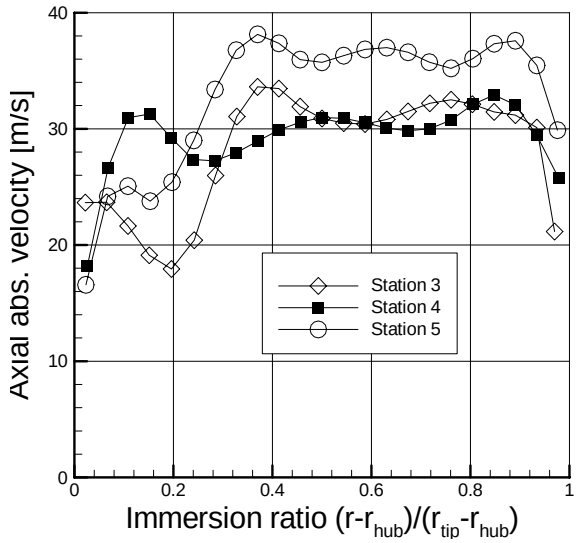

Figure 16 Radial distribution of axial velocity component, Cylindrical blades - 2600rpm.

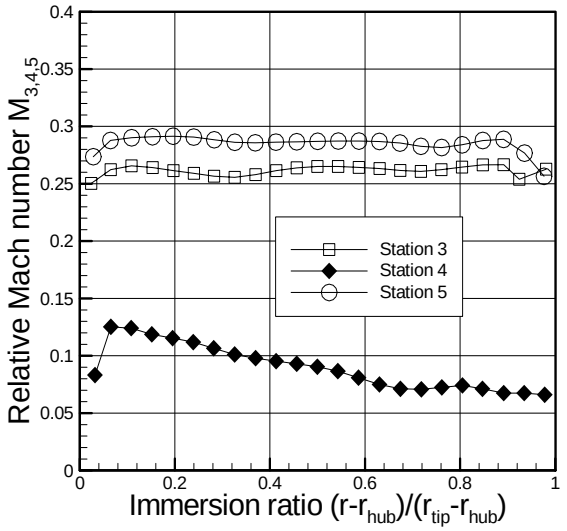

Figure 15 Radial distribution of relative Mach number, 3-D Bowed blades - 2600rpm.

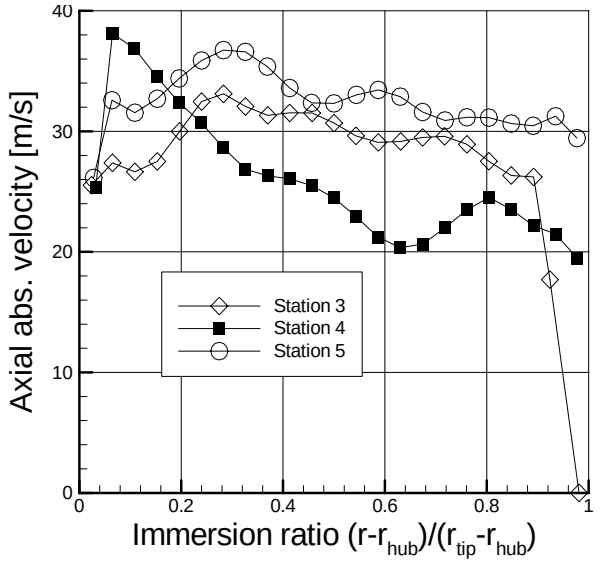

Figure 17 Radial distribution of axial velocity component, 3-D Bowed blades - 2600rpm.

The axial velocities again decrease near the tip (after r*=0.85) for all three stations, influenced by the interaction of the main flow with the tip secondary flow. The blade mid section shows moderate variation indicating higher axial velocities and smaller secondary vortices. In contrast the 3-D bowed blades (Fig. 17) confront higher axial velocities very close to the rotor hub. These higher velocities stifle the production of low energy vortices, prominent in the conventional cylindrical blades, which cause a higher drag induced force on the blades and add to the secondary losses. Along stations 3 and 5 the axial velocities reduce slightly as we move radially towards the blade tip while at station 4, a large axial velocity drop is seen after the initial high velocities.

Relative total pressure loss coefficient

Relative total pressure loss coefficient, $\zeta/\zeta_{0.5}$, for the two blade geometries and the stator and rotor stages are as shown in figs. 18 and 19 with ζ the loss coefficient at each radial location and $\zeta_{0.5}$ the loss coefficient at r*=50%. Using the consistently averaged circumferential quantities, the relative loss coefficient for stator and rotor are defined as:

$$\zeta_{Stator} = \frac{P_3 - P_4}{P_3 - p_4} \qquad \zeta_{Rotor} = \frac{P_{4r} - P_{5r}}{P_{4r} - p_5} \qquad (2)$$

with P_3 and P_4 as the absolute total pressure upstream and downstream of the stator, $(P_{4r}-P_{5r})$ as the relative total pressure upstream and downstream of the rotor, and P_4, P_5

as the static pressure at station 4 and 5. A comparison between the graphs for the two blades in general show a higher loss coefficient for the cylindrical blades all along the radial direction for the rotor and stator stages. As expected the losses for the cylindrical blades are even higher near the hub and tip regions than along the blade mid-section. For the cylindrical blades (Fig. 18), the losses are the lowest between r*=0.3 and 0.6 for the rotor as well as the stator stages. The pressure losses near the hub and tip regions are 2 to 3 times larger than what is observed for the 3-D bowed blades in the same zone. On the whole the relative total pressure loss for the 3-d bowed blade is very low and also uniform for almost 90% of the blade length.

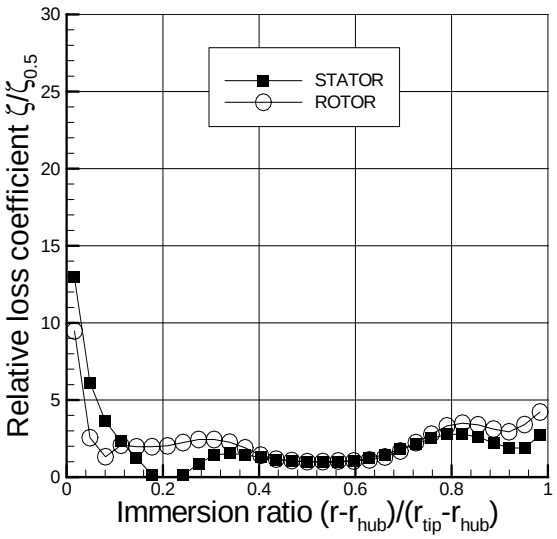

Figure 18 Radial distribution of relative loss coefficient, Cylindrical blades - 2600rpm.

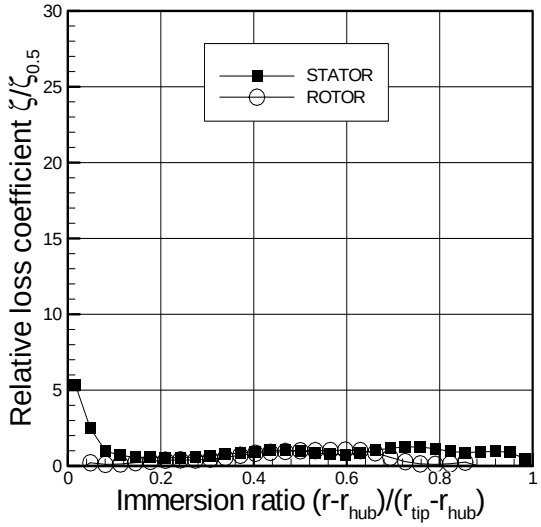

Figure 19 Radial relative loss distribution, 3-D Bowed blades - 2600rpm.

Qualitative comparison with the earlier investigations by Berg [14] and the very recent study by Emund et al. [15] show that the implementation of a 3-D configuration design reduced the secondary flow losses considerably. Berg in his study, which is probably one of the most comprehensive studies concerning the secondary flow losses in HP-turbine blades, used a series of cylindrical blades for his secondary flow loss investigations. His loss coefficient plots show two very pronounced peaks located at 18% and 85% of the blade span for all five rotors he investigated. The low total pressure regions occupied by the secondary flow losses

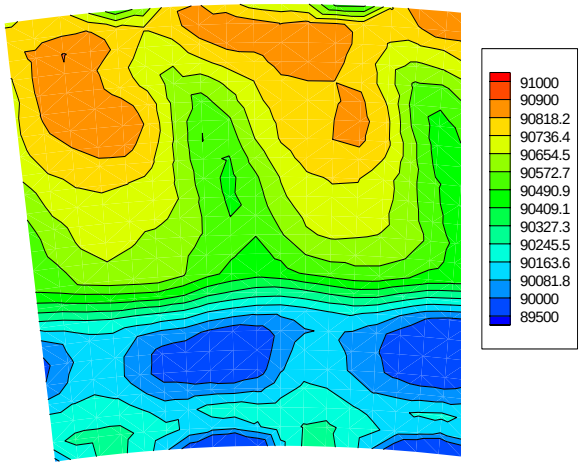

Figure 20 Total pressure contour at station 3, Cylindrical blades - 2600rpm.

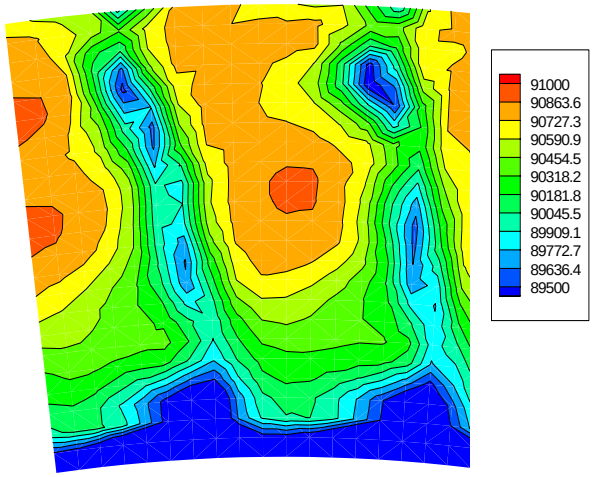

Figure 21 Total pressure contour at station 4, Cylindrical blades - 2600rpm

extend from 0% to 30% at the hub and from 80% to 100% at the tip. Similar distributions are found in many LPT-studies such as the one by Schütz [16]. Emund et al. used Traupel and VKI profiles, which are untwisted blades, for their 1.5-stage investigations. Although Emund et al. have not presented the total pressure loss coefficients, their

spanwise total pressure distributions exhibit a similar picture as found by Berg.

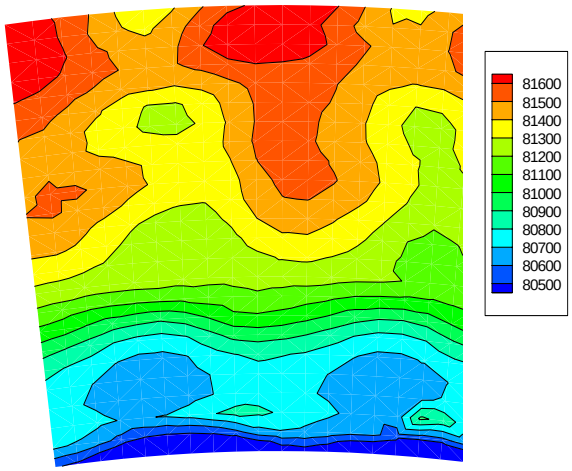

Figure 22 Total pressure contour at station 5, Cylindrical blades - 2600rpm.

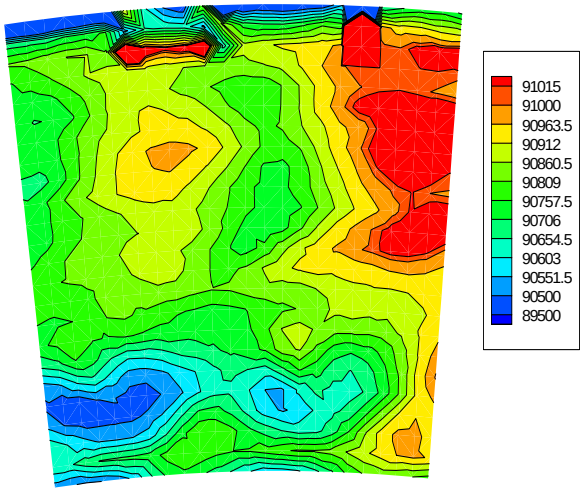

Figure 23 Total pressure contour at station 3, 3-D Bowed blades - 2600rpm.

Total pressure contours at each station

The total pressure contour plots for the cylindrical blades are shown in Figs. 20, 21 and 22. For station 3 (Fig. 20), large patches of low pressures are clearly visible near the hub up to 40% of the blade radial distance. This is primarily due to the secondary flow losses near the hub region. Low pressure zones are also noticed all along the blade further contributing to the pressure loss observed in Fig. 19. Station 4 (Fig. 21) shows a thinner low pressure low energy flow region than station 3 close to the hub. A relatively thick wake is noticed downstream of the stator blade trailing edge due to high secondary flows along the blade and also due to the inherent profile losses. The total pressure contour at station 5 (Fig. 22) is identical to that seen for station 3 with the low and high pressures occurring at almost similar locations.

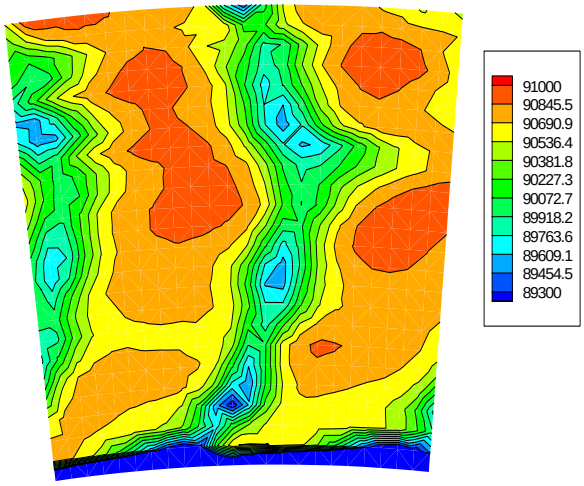

Figure 24 Total pressure contour at station 4, 3-D Bowed blades.

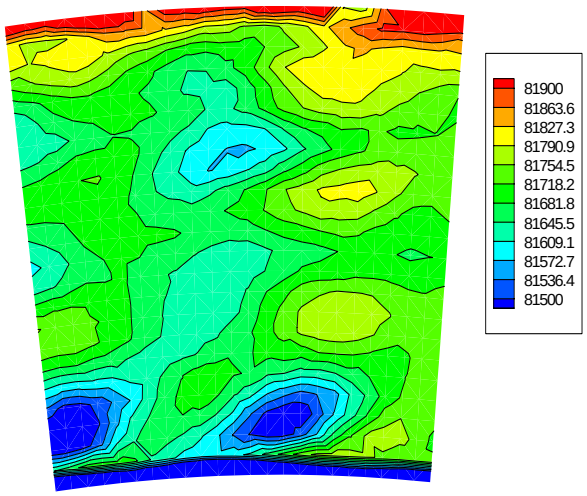

Figure 25 Total pressure contour at station 5, 3-D Bowed blades - 2600rpm

Figs. 23, 24 and 25 show the total pressure contour plots at stations 3,4 and 5 for the 3-D bowed blades. It is seen that the total pressures near the hub and the blade tip for station 3 (Fig. 23) are considerably higher than for the cylindrical blades. The higher total pressures are more widely distributed indicating that the extent of the secondary flow region is substantially reduced. Station 4 (Fig. 24) has a smaller pressure loss at the hub and along the blade than station 3. A distinct blade wake comparable to that for the cylindrical blades is observed at the same station, except that for the 3-d bowed blades the higher pressures are more wide spread. The higher magnitudes near the blade hub for the 3-d bowed blade at station 4 also implies that the losses are smaller in comparison to the cylindrical blades. Again Station 5 (Fig. 25) exhibits a similar total pressure distribution as station 3, but with a lower pressure level. A comparison of the total pressure distribution at each station for the two blades clearly shows lower pressures more

widely prevalent for the cylindrical blades indicating higher total pressure losses than for the 3-D blades.

CONCLUSIONS

A comparative study was performed to quantify the impact of blade geometry on secondary flow losses. The three stage HP- pressure research turbine facility at the Turbine Performance and Flow Research Laboratory, Texas A&M University was used for the current investigation. Two rotors with identical hub and tip diameters but with cylindrical and 3-D bowed blading were used to carry out aerodynamics and performance measurements. Interstage measurements upstream of the second stator, up- and downstream of the second rotor were performed. Detailed radial and circumferential traverse of the interstage flow field provided a clear picture about the total pressure distribution for both the blade types. The results clearly indicated that the 3-D blade configuration effectively reduced the extent of the secondary flow region compared to the one generated by the cylindrical blades. This resulted in a decrease of the secondary flow losses thus, increasing the stage efficiency. The study suggests that, there is real potential for further reducing the secondary flow losses by optimizing the blade lean and the convexity. An "S" shaped blade geometry that might result from an optimization process would probably be the direction to pursue in future development.

ACKNOWLEDGMENTS

The research reported in this paper was supported by the Siemens-Westinghouse Power Corporation. The authors would like to thank Dr. Chen. Mr. Martin, Mr. Pallotta and the Siemens-Westinghouse Power Corporation.

REFERENCES

[1] Arndt, N., 1993, Blade Row Interaction in a Multistage Low Pressure Turbine," ASME, *Journal of Turbomachinery*, Vol. 115, pp. 137-146.

[2] Sieverding, C. H., 1985, "Recent Progress in the Understanding of Basic Aspects of Secondary Flows in Turbine Blade Passages," ASME, *Journal of Turbomachinery*, 107, pp. 248-257.

[3] Bindon, J. P., 1989, "The Measurement and Formation of Tip Clearance Loss," ASME, *Journal of Turbomachinery*, 111, pp. 257-263.

[4] Chana K. S., Jones T. V., 2003, "An Investigation on Turbine Tip and Shroud Heat Transfer," ASME *Journal of Turbomachinery*, 125, pp. 513-520.

[5] Schobeiri M. T., Gillaranz J. L., Johansen E. S., 2000, "Aerodynamic and Performance Studies of a Three Stage High Pressure Research Turbine with 3-D Blades, Design Point and Off-Design Experimental Investigations," Proceedings of ASME TurboExpo 2000, 2000-GT-484.

[6] Aunapu N. V., Volino R. J., Flack K. A., Stoddard R. M.,2000, "Secondary Flow Measurements in a Turbine Passage with Endwall Flow Modification," ASME, *Journal of Turbomachinery*, 122, pp. 651-658.

[7] Prasad A., Wagner J. H., 2000, "Unsteady Effects in Turbine tip Clearance Flows,"ASME, *Journal of Turbomachinery*, 122, pp. 621-627.

[8] Camci C., Dey D., Kavurmacioglu L., 2003, "Tip Leakage Flows Near Partial Squealer Rims in an Axial Flow Turbine Stage," Proceedings of ASME TurboExpo 2003, Power of Land, Sea and Air, GT2003-38979.

[9] Chaluvadi V. S. P., Kalfas A. I., Hodson H. P., 2003, " Vortex Transport and Blade Interactions in High Pressure Turbines," Proceedings of ASME TurboExpo 2003, Power of Land, Sea and Air, GT2003-38389.

[10] Staubach, J. B., Sharma , O. P. and Stetson G. M., " Reduction of Tip Clearance Losses through 3D Aerofoil Design," ASME, 1996.

[11] Walker P. J., " Influence of Blade Lean in Axial Turbines: Model Turbine Measurements and Simulation by Novel Numerical Method," PhD Thesis, Cambridge University, 1989.

[12] Denton J. D. and Xu .L, 1999, "Exploitation of Three Dimensional Flow in Turbomachinery Design," Developments in Turbomachinery Design, Professional Engineering Publishing, pp. 121-133

[13] Dzung. L. S., 1971, "Konsisstente Mittewerte in der Theorie der Turbomaschinen fur Kompressible medien," BBC Mitteilung 58, 1971, 485-492.

[14] Berg, H..,1973, "Untersuchungen über den Einfluß der Leistungszahl auf Verlusten in Axialturbinen, Dissertation, Facultät Maschinenbau, Technische Hochschule Darmstadt, D17.

[15] Emunds R., Jennions I. K., Bohn D., Gier J., 1999, "Computation of Adjacent Blade-Row Effects in a 1.5-Stage Axial Flow Turbine," ASME,*Journal of Turbomachinery*, 121, pp. 1-10.

[16] Schütz, J, 1971, "Beitrag zur Berechnung der Strömung in Stufen axialer thermischer Turbomaschinen, Dissertation, Facultät Maschinenbau, Technische Hochschule Darmstadt, D17.